physics

IMPACT FACTOR 1.5

CITESCORE 3.0

Article

Performance Analysis for High-Dimensional Bell-State Quantum Illumination

Jeffrey H. Shapiro

MDPI

https://doi.org/10.3390/physics7010007

physics

MDPI

Article

Performance Analysis for High-Dimensional Bell-State Quantum Illumination

Jeffrey H. Shapiro

Research Laboratory of Electronics, Massachusetts Institute of Technology, Cambridge, MA 02139, USA; jhs@mit.edu

Abstract: Quantum illumination (QI) is an entanglement-based protocol for improving LiDAR/radar detection of unresolved targets beyond what a classical LiDAR/radar of the same average transmitted energy can do. Originally proposed by Seth Lloyd as a discrete-variable quantum LiDAR, it was soon shown that his proposal offered no quantum advantage over its best classical competitor. Continuous-variable, specifically Gaussian-state, QI has been shown to offer a true quantum advantage, both in theory and in table-top experiments. Moreover, despite its considerable drawbacks, the microwave version of Gaussian-state QI continues to attract research attention. A recent QI study by Armanpreet Pannu, Amr Helmy, and Hesham El Gamal (PHE), however, has: (i) combined the entangled state from Lloyd's QI with the channel models from Gaussian-state QI; (ii) proposed a new positive operator-valued measurement for that composite setup; and (iii) claimed that, unlike Gaussian-state QI, PHE QI achieves the Nair–Gu lower bound on QI target-detection error probability at all noise brightnesses. PHE's analysis was asymptotic, i.e., it presumed infinite-dimensional entanglement. The current paper works out the finite-dimensional performance of PHE QI. It shows that there is a threshold value for the entangled-state dimensionality below which there is no quantum advantage, and above which the Nair–Gu bound is approached asymptotically. Moreover, with both systems operating with error-probability exponents 1 dB lower than the Nair–Gu bound, PHE QI requires enormously higher entangled-state dimensionality than does Gaussian-state QI to achieve useful error probabilities in both high-brightness (100 photons/mode) and moderate-brightness (1 photon/mode) noise. Furthermore, neither system has an appreciable quantum advantage in low-brightness (much less than 1 photon/mode) noise.

Keywords: quantum radar; quantum illumination; two-mode squeezed-vacuum states

Received: 27 November 2024
Revised: 8 January 2025
Accepted: 5 February 2025
Published: 3 March 2025

Citation: Shapiro, J.H. Performance Analysis for High-Dimensional Bell-State Quantum Illumination. *Physics* **2025**, *7*, 7. https://doi.org/10.3390/physics7010007

1. Introduction

LiDAR (at optical wavelengths) and radar (at microwave wavelengths) transmit electromagnetic radiation into a region of interest to discern characteristics of objects, which may or may not be present therein, based on the return radiation collected from that region [1]. Despite electromagnetic radiation being fundamentally quantum mechanical [2], it is only recently that the use of quantum resources, specifically entanglement, has been considered for improving the performance of classical LiDARs or radars, i.e., those whose performance can be correctly assessed without treating their radiation in quantum terms. Of special note in regard to quantum LiDAR or radar is quantum illumination (QI), in which entangled signal and idler beams are created, with the signal transmitted into the region of interest, while the idler is retained for a joint measurement with the returned

radiation, see Refs. [3–5] for reviews of QI. Inasmuch as QI target detection is the present paper's focus, it behooves us to briefly delve into some relevant history.

Seth Lloyd [6] coined the term "quantum illumination" for a LiDAR that transmitted a sequence of M-mode single-photon states while retaining their maximally entangled single-photon companions for a joint measurement with the returned radiation. Lloyd assumed that the environment being probed never returned more than one photon in response to each transmission and that the returned photon was either background noise or a target reflection. Lloyd compared his QI performance with that of a single-photon (SP) LiDAR that probed the environment with the same state as his QI LiDAR, but had no stored idler. Lloyd argued that QI's entanglement would prevent a background photon from masquerading as the entangled companion of QI's stored idler. Indeed, as compared to SP target detection, Lloyd's QI target detection afforded a factor-of-M improvement in error-probability exponent in his high-noise regime, i.e., when it is highly probable that the returned radiation from a single transmission is due to background as opposed to target reflection. That said, Lloyd's QI and SP LiDARs are both quantum LiDARs, as they employ nonclassical transmitter states. Thus, when the author of this paper and Lloyd [7] compared Lloyd's QI with its best classical LiDAR counterpart, it turned out that the former could do no better than the latter and could perform much worse. As a result, interest in Lloyd's discrete-variable QI languished and was supplanted by interest in a continuous-variable version of QI, viz., Gaussian-state QI LiDAR by Si-Hui Tan and colleagues [8].

In Gaussian-state QI, M-mode pulses of quadrature-entangled signal and idler are produced, with the former probing the region of interest and the latter stored for a joint measurement with the returned radiation. For detecting the possible presence of a weakly reflecting target embedded in high-brightness (much more than 1 photon/mode) background radiation, Ref. [8] showed that Gaussian-state QI offered a 6 dB advantage in error-probability exponent over its best classical competitor of the same transmitted energy. Remarkably, this 6 dB performance advantage is obtained only in high-brightness noise, where the initial entanglement is destroyed, not in low-brightness (much less than 1 photon/mode) noise such as exists at optical wavelengths [9]. Consequently, intense interest in Gaussian-state QI did not develop until Ref. [10] showed how it could be used at microwave wavelengths, where weak target returns and high-brightness noise are the norm.

Initial table-top Gaussian-state QI experiments using sub-optimum receiver architectures have been reported for the optical region (with artificially injected high-brightness noise) [11], and for the microwave, [12]. Although these experiments only demonstrated roughly 20% signal-to-noise ratio gains over their best classical competitors, they did verify Gaussian-state QI's unique capability of providing an entanglement-based quantum advantage in an entanglement-breaking target-detection scenario. As explained in Refs. [3–5], Gaussian-state QI in the microwave faces enormous hurdles before its target-detection advantage can find a realistic use case. These include Gaussian-state QI's need to interrogate one resolution bin at a time; Gaussian-state QI's need for a quantum memory to store its high time–bandwidth product idler; Gaussian-state QI's requiring radiation with likely-to-be unattainably high time–bandwidth products; and Gaussian-state QI's requiring an interferometric measurement. The previous sentence emphasizes "Gaussian-state" because PHE's recently proposed discrete-variable QI [13] may avoid some of the problems that plague Gaussian-state QI.

Reference [13] does not assume that at most one photon is returned per transmission from the region being probed, hence avoiding the root cause of Lloyd's QI not outperforming its best classical competitor. Its analysis is asymptotic in that it passes to the limit $M \to \infty$ for the discrete-variable entangled state introduced in Lloyd's QI. Doing so drives the receiver's false-alarm probability to zero and makes it possible to prove that PHE QI

realizes 6 dB quantum advantage in error-probability exponent in high-brightness noise, matching both performance found by Tan and colleagues [8] in that regime and the Nair–Gu bound [14] on the attainable error-probability exponent of all possible QI protocols. Indeed, in this asymptotic regime, PHE QI matches the Nair–Gu bound at all noise brightnesses. However, contrary to Ref. [13]'s claim that Gaussian-state QI does not achieve Nair–Gu performance at low-noise brightness, it is easily shown that the system's error-probability exponent approaches the Nair–Gu bound, regardless of the noise brightness, as its signal brightness, N_S, is decreased. This demonstration can be accomplished either by evaluating the Chernoff bound for Gaussian-state QI as in Ref. [8] with $N_S \to 0$, or by modifying Ref. [15]'s binary phase-shift keying analysis for two-mode squeezed-vacuum (TMSV) communication to apply to on-off keying.

Requiring infinite entangled-state dimensionality, i.e., $M \to \infty$, puts PHE QI beyond the realm of practicality because it entails a transmission with infinite time-bandwidth product, and Ref. [13] presents no finite-M results for the error-probability exponent. The current paper remedies the preceding problem. In particular, it introduces a new, more explicit result for the joint density operator of the returned and retained radiation when the target is present. Using this result, accurate approximations to the single-shot false-alarm and detection probabilities are obtained for PHE QI. From those approximations, the finite-M multi-shot likelihood-ratio test can be obtained. The Chernoff bound can then be used to derive that test's error-probability exponent, which shows that PHE QI has "good" and "bad" regimes, analogous to those of Lloyd's QI. Moreover, only in the good regime—which requires M to exceed a threshold value—does PHE QI offer a quantum advantage for the error-probability exponent.

The rest of the paper is organized as follows. Section 2 presents the setup assumed in Ref. [13] and summarizes its key results. Section 3 derives the finite-M joint density operators for the returned and retained radiation under target absence and presence, with the latter being much more amenable to finite-M performance analysis than the form presented in Ref. [13]. Section 4 gives accurate approximations to the false-alarm and detection probabilities for a single finite-M transmission, which are then used in Section 5 to analyze multi-shot performance. Section 6 concludes the study with an appraisal of the results obtained and a comparison with Gaussian-state QI. Appendix A then contains derivation details for the target-present density operator, and Appendix B shows that the first-order corrections to Section 4's false-alarm and detection-probability approximations lead to inconsequential changes in those results.

2. Pannu–Helmy–El Gamal Quantum Illumination

PHE QI is an amalgam of Lloyd's QI and the Gaussian-state QI of Tan and colleagues. Thus, like Lloyd's QI transmitter, PHE QI's transmitter prepares a sequence of M-dimensional, signal-idler (SI) high-dimensional Bell states,

$$|\psi\rangle_{SI} = \frac{1}{\sqrt{M}} \sum_{m=1}^{M} |\mathbf{e}_m\rangle_S \, |\mathbf{e}_m\rangle_I, \tag{1}$$

where, for $K = S, I$, $|\mathbf{e}_m\rangle_K$ denotes an M-mode Fock state for modes with annihilation operators $\{\hat{a}_{K_m} : 1 \leq m \leq M\}$ containing 1 photon in mode m and no photons in the remaining modes. Again, like Lloyd's QI, PHE QI transmits the signal modes from Equation (1) into the region of interest and retains the idler modes for a subsequent joint measurement with the radiation returned therefrom. Using $\{\hat{a}_{R_m} : 1 \leq m \leq M\}$ to denote the annihilation operators for those M returned modes, PHE QI's channel models for target absence and

presence are those of Gaussian-state QI. Specifically, under hypothesis H_0 (target-absent), Ref. [13] uses

$$\hat{a}_{R_m} = \hat{a}_{B_m}, \tag{2}$$

where the $\{\hat{a}_{B_m} : 1 \leq m \leq M\}$ are annihilation operators for background-noise modes that are in independent, identically distributed (iid) thermal states with average photon number N_B. On the other hand, under hypothesis H_1 (target-present), Ref. [13] uses

$$\hat{a}_{R_m} = \sqrt{\kappa}\,\hat{a}_{S_m} + \sqrt{1-\kappa}\,\hat{a}_{B_m}, \tag{3}$$

where $\kappa \ll 1$ is the roundtrip transmissivity to and from the weakly reflecting target, and the iid background modes are now in thermal states with average photon number $N_B/(1-\kappa)$ to preclude the possibility of a passive signature of target presence. Strictly speaking, Ref. [13] only needs the noise modes to be in iid states with average photon numbers N_B and $N_B/(1-\kappa)$ for target absence and presence, respectively. It is assumed here that the iid noise states are thermal, which is the case for naturally occurring background radiation.

Reference [13]'s insight—the paper's principal novelty—lies in the PHE receiver's positive operator-valued measurement (POVM) for the returned and the retained-idler radiation from a single transmission. On each transmission, Lloyd's QI receiver uses the POVM

$$\hat{\Pi}_k = \begin{cases} |\psi\rangle_{RIRI}\langle\psi|, & \text{for } k = 1, \\ \hat{I}_{RI} - \hat{\Pi}_1, & \text{for } k = 0, \end{cases} \tag{4}$$

to decide H_k was true, where

$$|\psi\rangle_{RI} = \frac{1}{\sqrt{M}} \sum_{m=1}^{M} |\mathbf{e}_m\rangle_R\, |\mathbf{e}_m\rangle_I, \tag{5}$$

and $\hat{I}_{RI}$ is the identity operator on the state space of the $\{\hat{a}_{R_m}, \hat{a}_{I_m}\}$ modes. Instead, for each transmission, the PHE receiver uses the POVM

$$\hat{\Pi}_k = \begin{cases} \sum_{\mathbf{N}} |\psi_{\mathbf{N}}\rangle_{RIRI}\langle\psi_{\mathbf{N}}|, & \text{for } k = 1, \\ \hat{I}_{RI} - \hat{\Pi}_1, & \text{for } k = 0, \end{cases} \tag{6}$$

where $\mathbf{N} \equiv (N_1, N_2, \ldots, N_M)$, $\sum_{\mathbf{N}} \equiv \prod_{m=1}^{M} \sum_{N_m=0}^{\infty}$, and

$$|\psi_{\mathbf{N}}\rangle_{RI} \equiv \sum_{m=1}^{M} \sqrt{\frac{N_m + 1}{|\mathbf{N}| + M}}\, |\mathbf{e}_m + \mathbf{N}\rangle_R\, |\mathbf{e}_m\rangle_I, \tag{7}$$

with $|\mathbf{N}| \equiv \sum_{m=1}^{M} N_m$ and $|\mathbf{e}_m + \mathbf{N}\rangle_R$ being the returned modes' state containing $N_m + 1$ photons in the $\hat{a}_{R_m}$ mode and $N_{m'}$ photons in the $\{\hat{a}_{R_{m'}} : m' \neq m\}$ modes.

Note that $|\psi_{\mathbf{0}}\rangle_{RI} = |\psi\rangle_{RI}$, making PHE QI's POVM a natural generalization of Lloyd's POVM to the channel models of Gaussian-state QI, with their arbitrarily high numbers of photons in each returned mode. So, with $\hat{\rho}_{RI}^{(0)}$ being the joint density operator for the $\{\hat{a}_{R_m}, \hat{a}_{I_m}\}$ modes under hypothesis H_0, Ref. [13] shows that the M-mode, single-shot, false-alarm probability, $p_F \equiv \mathrm{Tr}(\hat{\Pi}_1 \hat{\rho}_{RI}^{(0)})$, goes to zero as $M \to \infty$. Similarly, it shows that the M-mode, single-shot, detection probability, $p_D \equiv \mathrm{Tr}(\hat{\Pi}_1 \hat{\rho}_{RI}^{(1)})$, obeys $\lim_{M\to\infty} p_D \geq \kappa/(N_B + 1)$, where $\hat{\rho}_{RI}^{(1)}$ is the joint density operator for the $\{\hat{a}_{R_m}, \hat{a}_{I_m}\}$ modes under hypothesis H_1. As the false-alarm probability vanishes in this limit, Ref. [13] finds that after $N_T \gg 1$ transmissions, the multi-shot miss probability satisfies

$$\lim_{M\to\infty} P_M \leq [1 - \kappa/(N_B + 1)]^{N_T} \approx e^{-\kappa N_T/(N_B+1)}, \tag{8}$$

where the approximation is valid because $\kappa \ll 1$. For equally likely target absence or presence, as assumed in this paper, the $M \to \infty$ multi-shot error probability then obeys

$$\Pr(e) \leq [1 - \kappa/(N_B + 1)]^{N_T}/2 \approx e^{-\kappa N_T/(N_B+1)}/2. \tag{9}$$

The Nair–Gu lower bound (LB) on QI error probability for equally likely target absence or presence when N_T signal photons are transmitted on average is [14]

$$\Pr(e)_{\text{LB}} \geq [1 - \kappa/(N_B + 1)]^{N_T}/4 \approx e^{-\kappa N_T/(N_B+1)}/4, \tag{10}$$

where the approximation uses $\kappa \ll 1$. (The factors of $1/2$ and $1/4$ appearing in Equations (9) and (10), respectively, are due to the former being, in essence, a Chernoff bound and the latter coming from a Helstrom bound.)

The Nair-Gu lower bound applies to optimum quantum reception for an arbitrary choice of the signal-idler state, subject only to the constraint on the average transmitted photon number. Comparing Equations (9) and (10) then shows that the PHE receiver achieves the ultimate error-probability exponent, in the limit $M \to \infty$, for weakly reflecting ($\kappa \ll 1$) targets at all noise brightnesses. Compared to its best classical competitor [7], viz., a coherent-state (CS) system transmitting N_T photons on average whose error-probability Chernoff bound is [8]

$$\Pr(e)_{\text{CS}} \leq e^{-\kappa N_T(\sqrt{1+N_B}-\sqrt{N_B})^2}/2, \tag{11}$$

PHE QI thus offers a 6 dB quantum advantage in error-probability exponent when $N_B \gg 1$, no appreciable quantum advantage when $N_B \ll 1$, and 4.6 dB quantum advantage at $N_B = 1$. Gaussian-state QI matches those behaviors because, as noted earlier, its error-probability exponent approaches the Nair–Gu bound in the limit of low signal brightness. See Section 6 for a more detailed appraisal of PHE QI versus Gaussian-state QI.

3. Joint Density Operators

The principal drawback of Ref. [13]'s treatment of PHE QI is the absence of any finite-M results for the error-probability exponent. This Section begins the task of obtaining such results by deriving a more useful form for the joint density operator for the single-shot returned and retained-idler radiation when the target is present. For completeness, however, its target-absent counterpart is presented first, as that will be needed to evaluate the finite-M, single-shot, false-alarm probability. From Equation (2) one immediately finds that

$$\hat{\rho}_{RI}^{(0)} = \hat{\rho}_B^{(0)} \otimes \hat{\rho}_I, \tag{12}$$

where

$$\hat{\rho}_B^{(0)} = \bigotimes_{m=1}^{M} \sum_{N_m=0}^{\infty} \frac{N_B^{N_m}}{(N_B+1)^{N_m+1}} |N_m\rangle_{R_m\,R_m}\langle N_m|, \tag{13}$$

with $|N_m\rangle_{R_m}$ being the N_m-photon state of the $\hat{a}_{R_m}$ mode, and

$$\hat{\rho}_I = \text{Tr}_S(|\psi\rangle_{SI\,SI}\langle\psi|) = \frac{1}{M}\sum_{m=1}^{M} |\mathbf{e}_m\rangle_{I\,I}\langle\mathbf{e}_m|. \tag{14}$$

To find the target-present joint density operator, $\hat{\rho}_{RI}^{(1)}$, a characteristic-function approach is used here to obtain its number–ket representation. The anti-normally ordered characteristic function associated with $\hat{\rho}_{RI}^{(1)}$ is

$$\chi_A^{\rho_{RI}^{(1)}}(\boldsymbol{\zeta}_R, \boldsymbol{\zeta}_I) \equiv \text{Tr}\Big(\hat{\rho}_{RI}^{(1)}\, e^{-\boldsymbol{\zeta}_R^*\cdot\hat{\mathbf{a}}_R - \boldsymbol{\zeta}_I^*\cdot\hat{\mathbf{a}}_I}\, e^{\boldsymbol{\zeta}_R\cdot\hat{\mathbf{a}}_R^\dagger + \boldsymbol{\zeta}_I\cdot\hat{\mathbf{a}}_I^\dagger}\Big), \tag{15}$$

where, for $K = R, I$, $\boldsymbol{\zeta}_K \equiv (\zeta_{K_1}, \zeta_{K_2}, \ldots, \zeta_{K_M})$ with $\{\zeta_{K_m}\}$ being complex valued, $\hat{\boldsymbol{a}}_K \equiv (\hat{a}_{K_1}, \hat{a}_{K_2}, \ldots, \hat{a}_{K_M})$, and $\hat{\boldsymbol{a}}_K^\dagger \equiv (\hat{a}_{K_1}^\dagger, \hat{a}_{K_2}^\dagger, \ldots, \hat{a}_{K_M}^\dagger)$. Using Equation (3), one can show that

$$\chi_A^{\rho_{RI}^{(1)}}(\boldsymbol{\zeta}_R, \boldsymbol{\zeta}_I) = \chi_A^{\rho_{SI}}(\sqrt{\kappa}\,\boldsymbol{\zeta}_R, \boldsymbol{\zeta}_I)\chi_A^{\rho_B^{(1)}}(\sqrt{1-\kappa}\,\boldsymbol{\zeta}_R), \tag{16}$$

where $\chi_A^{\rho_B^{(1)}}(\boldsymbol{\zeta}_B) \equiv \mathrm{Tr}\left(\hat{\rho}_B^{(1)} e^{-\boldsymbol{\zeta}_B^* \cdot \hat{\boldsymbol{a}}_B}\, e^{\boldsymbol{\zeta}_B \cdot \hat{\boldsymbol{a}}_B^\dagger}\right)$ is the anti-normally ordered characteristic function associated with $\hat{\rho}_B^{(1)}$. It is straightforwardly verified, using the assumed multi-mode thermal state for $\hat{\rho}_B^{(1)}$, that

$$\chi_A^{\rho_B^{(1)}}(\sqrt{1-\kappa}\,\boldsymbol{\zeta}_R) = e^{-\boldsymbol{\zeta}_R^* \cdot \boldsymbol{\zeta}_R (N_B + 1 - \kappa)}. \tag{17}$$

Next, to find $\chi_A^{\rho_{SI}}(\sqrt{\kappa}\,\boldsymbol{\zeta}_R, \boldsymbol{\zeta}_I)$, the Baker–Campbell–Hausdorff theorem [16] is first used to obtain

$$\chi_A^{\rho_{SI}}(\sqrt{\kappa}\,\boldsymbol{\zeta}_R, \boldsymbol{\zeta}_I) = e^{-\kappa \boldsymbol{\zeta}_R^* \cdot \boldsymbol{\zeta}_R - \boldsymbol{\zeta}_I^* \cdot \boldsymbol{\zeta}_I} \chi_N^{\rho_{SI}}(\sqrt{\kappa}\,\boldsymbol{\zeta}_R, \boldsymbol{\zeta}_I), \tag{18}$$

where

$$\chi_N^{\rho_{SI}}(\boldsymbol{\zeta}_S, \boldsymbol{\zeta}_I) \equiv \mathrm{Tr}\left(\hat{\rho}_{SI}\, e^{\boldsymbol{\zeta}_S \cdot \hat{\boldsymbol{a}}_S^\dagger + \boldsymbol{\zeta}_I \cdot \hat{\boldsymbol{a}}_I^\dagger}\, e^{-\boldsymbol{\zeta}_S^* \cdot \hat{\boldsymbol{a}}_S - \boldsymbol{\zeta}_I^* \cdot \hat{\boldsymbol{a}}_I}\right) \tag{19}$$

is the normally ordered characteristic function associated with $\hat{\rho}_{SI}$. Expanding Equation (19)'s exponential terms using their Taylor series and employing the result in Equation (18) makes it straightforward to evaluate Equation (18). Substituting the formula so obtained plus Equation (17) into Equation (16) gives us

$$\chi_A^{\rho_{RI}^{(1)}}(\boldsymbol{\zeta}_R, \boldsymbol{\zeta}_I) = e^{-\boldsymbol{\zeta}_R^* \cdot \boldsymbol{\zeta}_R (N_B + 1) - \boldsymbol{\zeta}_I^* \cdot \boldsymbol{\zeta}_I} \left(1 - \frac{\kappa \boldsymbol{\zeta}_R^* \cdot \boldsymbol{\zeta}_R}{M} - \frac{\boldsymbol{\zeta}_I^* \cdot \boldsymbol{\zeta}_I}{M} + \frac{\kappa |\boldsymbol{\zeta}_R \cdot \boldsymbol{\zeta}_I|^2}{M}\right). \tag{20}$$

Now it only remains to obtain the number–ket expansion of $\hat{\rho}_{SI}^{(1)}$ from that density operator's anti-normally ordered characteristic function via the operator-valued inverse Fourier transform,

$$\hat{\rho}_{RI}^{(1)} = \int \frac{\mathrm{d}^2 \boldsymbol{\zeta}_R}{\pi^M} \int \frac{\mathrm{d}^2 \boldsymbol{\zeta}_I}{\pi^M}\, \chi_A^{\rho_{RI}^{(1)}}(\boldsymbol{\zeta}_R, \boldsymbol{\zeta}_I) e^{-\boldsymbol{\zeta}_R \cdot \hat{\boldsymbol{a}}_R^\dagger - \boldsymbol{\zeta}_I \cdot \hat{\boldsymbol{a}}_I^\dagger}\, e^{\boldsymbol{\zeta}_R^* \cdot \hat{\boldsymbol{a}}_R + \boldsymbol{\zeta}_I^* \cdot \hat{\boldsymbol{a}}_I}, \tag{21}$$

where $\int \mathrm{d}^2 \boldsymbol{\zeta}_K / \pi^M \equiv \prod_{m=1}^M \int \mathrm{d}^2 \zeta_{K_m} / \pi$ for $K = R, I$, and integrals without limits are from $-\infty$ to ∞ in all their dimensions.

The rest of the derivation is rather involved, so it has been relegated to Appendix A. The final expression is

$$\begin{aligned}
\hat{\rho}_{RI}^{(1)} = {} & \frac{1}{M} \sum_{m=1}^M \sum_{\mathbf{N}} \left(\prod_{\ell=1}^M \frac{N_B^{N_\ell}}{(N_B+1)^{N_\ell+1}}\right)\left(1 - \frac{\kappa}{N_B+1} + \frac{\kappa N_m\, u(N_m-1)}{N_B(N_B+1)}\right) |\mathbf{N}\rangle_R\, |\mathbf{e}_m\rangle_{I\,I} \langle \mathbf{e}_m|_R \langle \mathbf{N}| \\
& + \frac{\kappa}{M} \sum_{\mathbf{N}} \sum_{\mathbf{N}'} \sum_{m=1}^M \sum_{\substack{m'=1 \\ m' \neq m}}^M \left(\prod_{\substack{\ell=1 \\ \ell \neq m, m'}}^M \frac{N_B^{N_\ell}\, \delta_{N_\ell N_\ell'}}{(N_B+1)^{N_\ell+1}}\right) \frac{N_B^{N_{m'}+N_m'}}{(N_B+1)^{N_{m'}+N_m'+4}} \sqrt{(N_{m'}+1)(N_m'+1)} \\
& \times \left(\bigotimes_{\substack{\ell=1 \\ \ell \neq m, m'}}^M |N_\ell\rangle_{R_\ell}\right) |N_m'+1\rangle_{R_m} |N_{m'}\rangle_{R_{m'}} |\mathbf{e}_m\rangle_{I\,I} \langle \mathbf{e}_{m'}|_{R_{m'}} \langle N_{m'}+1|_{R_m} \langle N_m'| \left(\bigotimes_{\substack{\ell=1 \\ \ell \neq m, m'}}^M {}_{R_\ell}\langle N_\ell'|\right),
\end{aligned} \tag{22}$$

where $u(\cdot)$ is the unit-step function and δ_{jk} is the Kronecker delta function.

4. Single-Shot False-Alarm and Detection Probabilities

The principal roadblock to obtaining finite-M results for the single-shot false-alarm and detection probabilities is the $1/\sqrt{|\mathbf{N}|+M}$ factor in $|\psi_{\mathbf{N}}\rangle_{RI}$. As $M \gg 1$ is necessary to achieve an acceptably low error probability for the assumed weakly reflecting target, especially in the case of high-brightness background noise, $|\mathbf{N}|+M$ will have high mean-to-standard-deviation ratios for all noise brightnesses under both the target-absent and target-present hypotheses. Thus, in this Section, $|\mathbf{N}|+M$ is replaced with its conditional means in evaluating p_F and p_D from Equation (6)'s POVM and Equations (12) and (22)'s joint density operators for target absence and presence. Appendix B shows that the first-order corrections to this Section's false alarm and detection-probability approximations are inconsequential.

To find the false-alarm probability approximation, let us first rewrite $\hat{\rho}_{RI}^{(0)}$ as

$$\hat{\rho}_{RI}^{(0)} = \sum_{\tilde{\mathbf{N}}} \Pr(\tilde{\mathbf{N}})\, |\tilde{\mathbf{N}}\rangle_R\, {}_R\langle\tilde{\mathbf{N}}| \otimes \frac{1}{M} \sum_{\tilde{m}=1}^{M} |\mathbf{e}_{\tilde{m}}\rangle_I\, {}_I\langle\mathbf{e}_{\tilde{m}}|, \tag{23}$$

where $\Pr(\tilde{\mathbf{N}}) \equiv \prod_{m=1}^{M} N_B^{\tilde{N}_m}/(N_B+1)^{\tilde{N}_m+1}$ and $|\tilde{\mathbf{N}}\rangle_R \equiv \bigotimes_{m=1}^{M} |\tilde{N}_m\rangle_{R_m}$. It then follows that

$$p_F = \sum_{\mathbf{N}} {}_{RI}\langle\psi_{\mathbf{N}}|\hat{\rho}_{RI}^{(0)}|\psi_{\mathbf{N}}\rangle_{RI} = \frac{1}{M} \sum_{\mathbf{N}} \sum_{\tilde{m}=1}^{M} \frac{N_{\tilde{m}}+1}{|\mathbf{N}|+M} \sum_{\tilde{\mathbf{N}}} \Pr(\tilde{\mathbf{N}})\, |{}_R\langle\mathbf{e}_{\tilde{m}}+\mathbf{N}|\tilde{\mathbf{N}}\rangle_R|^2. \tag{24}$$

Now, because

$$|{}_R\langle\mathbf{e}_{\tilde{m}}+\mathbf{N}|\tilde{\mathbf{N}}\rangle_R|^2 = \delta_{\tilde{N}_{\tilde{m}}(N_{\tilde{m}}+1)} \prod_{\substack{m'=1 \\ m'\neq m}}^{M} \delta_{\tilde{N}_{m'}N_{m'}}, \tag{25}$$

Equation (24) reduces to

$$p_F = \frac{1}{M} \sum_{\tilde{m}=1}^{M} \sum_{\tilde{\mathbf{N}}} \Pr(\tilde{\mathbf{N}}) \frac{\tilde{N}_{\tilde{m}}}{|\tilde{\mathbf{N}}|+M-1} \approx \frac{N_B}{M(N_B+1)-1}, \tag{26}$$

where the approximation uses

$$\frac{1}{|\tilde{\mathbf{N}}|+M-1} \approx \frac{1}{\sum_{\tilde{\mathbf{N}}} \Pr(\tilde{\mathbf{N}})(|\tilde{\mathbf{N}}|+M-1)} = \frac{1}{M(N_B+1)-1}. \tag{27}$$

Note that this p_F approximation vanishes for $M \to \infty$, as found in Ref. [13].

Turning to the single-shot detection probability, the starting point is

$$p_D = \sum_{\tilde{\mathbf{N}}} {}_{RI}\langle\psi_{\tilde{\mathbf{N}}}|\hat{\rho}_{RI}^{(1)}|\psi_{\tilde{\mathbf{N}}}\rangle_{RI} \tag{28}$$

$$= \sum_{\tilde{\mathbf{N}}} \sum_{m=1}^{M} \sum_{m'=1}^{M} \frac{\sqrt{(\tilde{N}_m+1)(\tilde{N}_{m'}+1)}}{|\tilde{\mathbf{N}}|+M} {}_I\langle\mathbf{e}_m|\, {}_R\langle\mathbf{e}_m+\tilde{\mathbf{N}}|\hat{\rho}_{RI}^{(1)}|\, |\mathbf{e}_{m'}+\tilde{\mathbf{N}}\rangle_R\, |\mathbf{e}_{m'}\rangle_I. \tag{29}$$

To proceed further the $m = m'$ and $m \neq m'$ components of Equation (29) are calculated separately, using, respectively, the first line and second-plus-third lines of Equation (22). For the $m = m'$ terms, one obtains

$$p_D^{(m=m')} = \frac{1}{M}\sum_{\tilde{\mathbf{N}}}\sum_{m=1}^{M}\frac{\tilde{N}_m+1}{|\tilde{\mathbf{N}}|+M}\left(\prod_{\substack{\ell=1\\ \ell\neq m}}^{M}\frac{N_B^{\tilde{N}_\ell}}{(N_B+1)^{\tilde{N}_\ell+1}}\right)\frac{N_B^{\tilde{N}_m+1}}{(N_B+1)^{\tilde{N}_m+2}}$$
$$\times\left(1-\frac{\kappa}{N_B+1}+\frac{\kappa(\tilde{N}_m+1)}{N_B(N_B+1)}\right) \tag{30}$$
$$\approx \frac{1}{M}\sum_{m=1}^{M}\sum_{\tilde{N}_m=0}^{\infty}\frac{\tilde{N}_m+1}{M(N_B+1)}\frac{N_B^{\tilde{N}_m+1}}{(N_B+1)^{\tilde{N}_m+2}}\left(1-\frac{\kappa}{N_B+1}+\frac{\kappa(\tilde{N}_m+1)}{N_B(N_B+1)}\right) \tag{31}$$
$$= \frac{\kappa+N_B}{M(N_B+1)}, \tag{32}$$

where the approximation uses

$$\frac{1}{|\tilde{\mathbf{N}}|+M} \approx \frac{1}{\sum_{\tilde{\mathbf{N}}}\left(\prod_{m=1}^{M}\frac{N_B^{\tilde{N}_m}}{(N_B+1)^{\tilde{N}_m+1}}\right)(|\tilde{\mathbf{N}}|+M)} = \frac{1}{M(N_B+1)}. \tag{33}$$

For the $m \neq m'$ terms the result is

$$p_D^{(m\neq m')} = \frac{\kappa}{M}\sum_{m=1}^{M}\sum_{\substack{m'=1\\ m'\neq m}}^{M}\sum_{\tilde{N}_m=0}^{\infty}\sum_{\tilde{N}_{m'}=0}^{\infty}\frac{N_B^{\tilde{N}_m+\tilde{N}_{m'}}}{(N_B+1)^{\tilde{N}_m+\tilde{N}_{m'}+4}}\frac{(\tilde{N}_m+1)(\tilde{N}_{m'}+1)}{|\tilde{\mathbf{N}}|+M} \tag{34}$$
$$\approx \frac{\kappa(M-1)}{M(N_B+1)}. \tag{35}$$

where the approximation uses Equation (33).

Putting the $m = m'$ and $m \neq m'$ results together gives the following approximation for the single-shot detection probability:

$$p_D \approx \frac{\kappa}{N_B+1}+\frac{N_B}{M(N_B+1)}. \tag{36}$$

5. Multi-Shot Likelihood Ratio and Error-Probability Exponent

In this Section, Equations (26) and (36) are first used to determine the multi-shot likelihood-ratio test (LRT) for minimum error-probability choice between equally likely target absence or presence based on the results of $N_T \gg 1$ PHE single-shot POVMs. From that LRT, the Chernoff bound is used to obtain its finite-M error-probability exponent, from which the dimensionality threshold that must be exceeded for there to be any quantum advantage can be identified, and the minimum dimensionality required to be within 1 dB of the Nair–Gu error-probability exponent can be obtained.

Let $\{d_n : 1 \leq n \leq N_T\}$ denote single-shot POVM results, i.e., $d_n = 1$ indicates a target-present decision on the nth transmission and $d_n = 0$ denotes a target-absent decision on that transmission. Conditioned on the true hypothesis, the $\{d_n\}$ are iid Bernoulli random variables with success probabilities p_F for H_0 and p_D for H_1. The LRT being sought here is therefore

$$\frac{\prod_{n=1}^{N_T} p_D^{d_n}[1-p_D]^{1-d_n}}{\prod_{n=1}^{N_T} p_F^{d_n}[1-p_F]^{1-d_n}} \underset{\text{decide } H_0}{\overset{\text{decide } H_1}{\gtrless}} 1, \tag{37}$$

which can be rewritten as

$$\frac{\left(\begin{array}{c} N_T \\ D_{N_T} \end{array} \right) p_D^{D_{N_T}} [1-p_D]^{N_T - D_{N_T}} \underset{\text{decide } H_0}{\overset{\text{decide } H_1}{\gtrless}} \left(\begin{array}{c} N_T \\ D_{N_T} \end{array} \right) p_F^{D_{N_T}} [1-p_F]^{N_T - D_{N_T}}}{} 1, \tag{38}$$

with

$$\left(\begin{array}{c} N_T \\ D_{N_T} \end{array} \right) \equiv \frac{N_T!}{D_{N_T}!(N_T - D_{N_T})!} \tag{39}$$

being the binomial coefficient and $D_{N_T} \equiv \sum_{n=1}^{N_T} d_n$.

Equation (38) shows that D_{N_T} is a sufficient statistic for the minimum error-probability test, and the D_{N_T}-based LRT can be reduced to the quite simple threshold test,

$$D_{N_T} \underset{\text{decide } H_0}{\overset{\text{decide } H_1}{\gtrless}} \frac{N_T \ln\{[1-p_F]/[1-p_D]\}}{\ln\{p_D[1-p_F]/p_F[1-p_D]\}}, \tag{40}$$

where M is assumed to be large enough that $p_D > p_F$, i.e.,

$$M > M_0 \equiv \frac{\kappa + \sqrt{\kappa^2 + 4\kappa N_B(N_B+1)}}{2\kappa(N_B+1)}. \tag{41}$$

The Chernoff bound of interest is

$$\Pr(e) \leq \Pr(e)_{\text{CB}} \equiv \min_{0 \leq s \leq 1} \sum_{n=0}^{N_T} \Pr(D_{N_T} = n \mid H_1)^s \Pr(D_{N_T} = n \mid H_0)^{1-s}/2. \tag{42}$$

For $M > M_0$, two straightforward calculations show that Equation (42) reduces to

$$\Pr(e) \leq \Pr(e)_{\text{CB}} = \min_{0 \leq s \leq 1} [p_D^s p_F^{1-s} + (1-p_D)^s (1-p_F)^{1-s}]^{N_T}/2, \tag{43}$$

and s_o, the minimizing s value, is

$$s_o = \frac{\ln\{[p_F/(1-p_F)]\ln[(p_D/p_F)]/\ln[(1-p_F)/(1-p_D)]\}}{\ln[(1-p_D)p_F/(1-p_F)p_D]}. \tag{44}$$

To quantify PHE QI's approach to the Nair–Gu lower bound on QI's error-probability exponent, let us introduce the penalty function $\mathcal{E}(\kappa, N_B, M)$ that satisfies

$$\exp\{-[\kappa N_T/(N_B+1)]\mathcal{E}(\kappa, N_B, M)\} = [p_D^{s_o} p_F^{1-s_o} + (1-p_D)^{s_o}(1-p_F)^{1-s_o}]^{N_T}, \tag{45}$$

and focus attention on two special cases, $\kappa = 0.001$ with $N_B = 100$ and $\kappa = 0.001$ with $N_B = 1$, as representatives of a weakly reflecting embedded in either high-brightness or moderate-brightness noise. In the high-brightness case the Nair–Gu bound gives 6 dB quantum advantage, and in the moderate-brightness case that bound gives 4.6 dB quantum advantage. For $N_B = 0.01$ low-brightness noise, the Nair–Gu bound gives 0.82 dB quantum advantage. Thus, a system operating 1 dB away from that bound offers no quantum advantage.

One can verify that $\lim_{M\to\infty} \mathcal{E}(\kappa, N_B, M) = 1$, so that the error-probability exponent, $-\log[2\Pr(e)_{\mathrm{CB}}]$, matches the Nair–Gu bound at infinite M, as shown in Ref. [13]. However, how high must M be to approach that limit? Figure 1 shows $\mathcal{E}(\kappa, N_B, M)$ versus $\log_{10}(M)$ for the representative cases, and Table 1 lists some key values therefrom. For the high-brightness noise, one can see that: (i) below the $M = 7.34 \times 10^5$ threshold, PHE QI offers no quantum advantage in error-probability exponent; and (ii) $M = 2.27 \times 10^{13}$ is necessary for PHE QI's error-probability exponent to be 1 dB lower than the Nair–Gu bound. Similarly, for the moderate-brightness noise, one finds that: (i) below the $M = 7.33 \times 10^3$ threshold, PHE QI offers no quantum advantage in error-probability exponent; and (ii) $M = 2.21 \times 10^{11}$ is necessary for PHE QI's error-probability exponent to be 1 dB lower than the Nair–Gu bound.

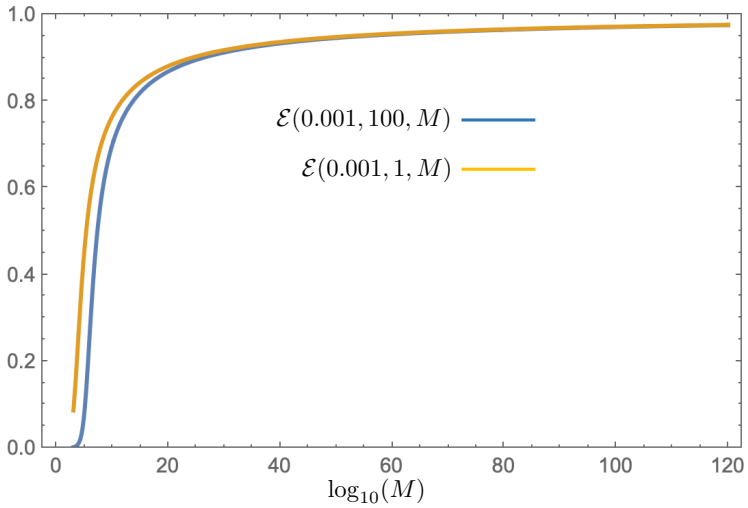

Figure 1. The penalty functions $\mathcal{E}(0.001, 1, M)$ (top curve) and $\mathcal{E}(0.001, 100, M)$ (bottom curve) versus $\log_{10}(M)$. Note that for both curves, the M values shown here exceed the penalty functions' M_0 thresholds for $p_D > p_F$, viz., 22.6 for the moderate-brightness noise, and 31.5 for the high-brightness noise. See text for details.

Table 1. M values needed for representative values of $\mathcal{E}(0.001, 100, M)$ and $\mathcal{E}(0.001, 1, M)$. See text for details.

M	$\mathcal{E}(0.001, 100, M)$	Comment
2.27×10^{13}	$10^{-0.1}$	1 dB off Nair–Gu bound
7.34×10^5	0.25	no quantum advantage
M	$\mathcal{E}(0.001, 1, M)$	Comment
2.21×10^{11}	$10^{-0.1}$	1 dB off Nair–Gu bound
7.33×10^3	0.25	no quantum advantage

6. Conclusions and Discussion

Reference [13] launched a new paradigm for discrete-variable QI target detection. First it combined the M mode-pair signal-idler state from Lloyd's QI with the low-transmissivity channel models from Tan and colleagues' Gaussian-state QI. Then it introduced a new single-shot POVM that enables the Nair–Gu bound on QI's error-probability exponent to be achieved at all noise brightnesses in the limit $M \to \infty$. The present paper has established the finite-M performance of PHE QI, showing that it has good and bad regimes—dictated by their entangled-state dimensionality—that are analogous to those of Lloyd's QI. Furthermore, for any combination of roundtrip target transmissivity and background-noise brightness, the current paper's finite-M results allow the entangled-state dimensionality needed to approach the Nair–Gu bound on QI's error-probability exponent to be quantified.

At this juncture, a comparison between finite-M PHE QI and Gaussian-state QI is warranted. Both systems can match the Nair–Gu bound on target-detection error-probability exponent for a weakly reflecting ($\kappa \ll 1$) target embedded in thermal noise. Moreover, neither offers any appreciable quantum advantage for low-brightness ($N_B \ll 1$) background noise. That said, the conditions required for each of these protocols to realize their respective quantum advantages are quite different.

Consider PHE QI and Gaussian-state QI for the $\kappa = 0.001$ with $N_B = 100$ and $\kappa = 0.001$ with $N_B = 1$ examples considered here, with both systems operating at error-probability exponents 1 dB lower than the Nair–Gu bound. In the high-brightness noise, PHE QI requires $M = 2.27 \times 10^{13}$ to operate at 1 dB below the Nair–Gu error-probability exponent, and achieves the Chernoff-bound performance shown in Figure 2, whereas in the moderate-brightness noise $M = 2.21 \times 10^{11}$ suffices for those purposes. Gaussian-state QI, on the other hand, requires the signal brightness to be $N_S = 0.01523$ to operate at 1 dB below the Nair–Gu bound in the high-brightness noise, whereas $N_S = 0.01421$ suffices for that purpose in the moderate-brightness noise. In both of those cases, it achieves Figure 2's Chernoff-bound performance, where $N_T = MN_S$ is now the average number of transmitted signal photons.

Figure 3 compares the entanglement dimensionalities of the two QI systems for the parameters used in Figure 2. Here, one sees that PHE QI requires more than 10^5 times the dimensionality that suffices for Gaussian-state QI in the high-brightness noise and more than 10^4 times the dimensionality that Gaussian-state QI requires in the moderate-brightness noise.

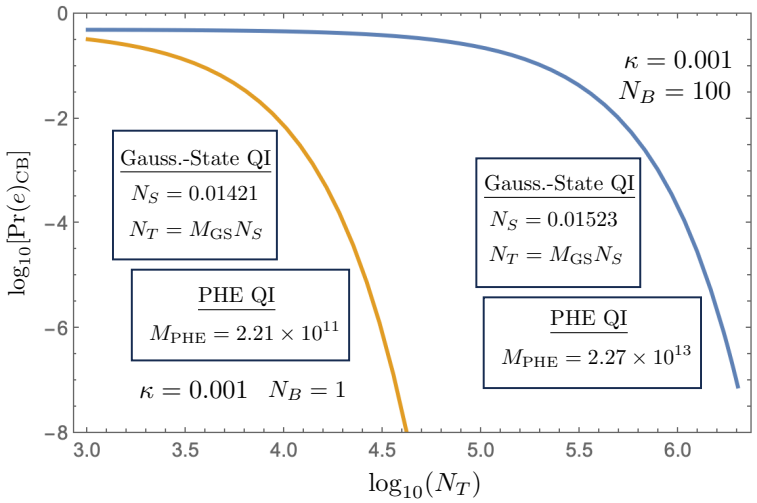

Figure 2. The Chernoff bound, $\Pr(e)_{\mathrm{CB}}$, versus N_T for PHE QI and Gaussian-state (GS) QI, as labelled, for $\kappa = 0.001$ with $N_B = 100$ (top curve) and $\kappa = 0.001$ with $N_B = 1$ (bottom curve), with both systems are operating at 1 dB below the Nair–Gu error-probability exponent. In the high-brightness noise, PHE QI requires $M = 2.27 \times 10^{13}$ to reach this operating point, whereas, in the moderate-brightness noise, $M = 2.21 \times 10^{11}$ suffices for this purpose. In both brightnesses, N_T is the number of transmitted signal photons. For Gaussian-state QI, this operating point requires $N_S = 0.01523$ in the high-brightness noise and $N_S = 0.01421$ in the moderate-brightness noise. In both of these cases, N_T is now the average number of transmitted signal photons. See text for details.

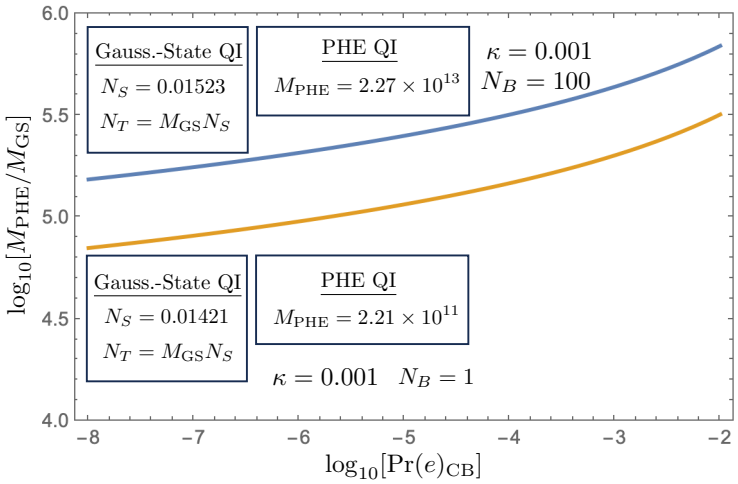

Figure 3. $M_{\rm PHE}/M_{\rm GS}$ versus $\Pr(e)_{\rm CB}$ where $M_{\rm PHE}$ and $M_{\rm GS}$ are the entangled-state dimensionalities associated with the $\Pr(e)_{\rm CB}$ versus N_T curves from Figure 2.

As if PHE QI's requiring 10^4-to-10^5 times the entangled-state dimensionality of Gaussian-state QI to achieve the same error probability were not bad enough, it incurs an even larger disadvantage when one looks at the time–bandwidth product. In the scalar-wave, unresolved-target scenario that being considered here, only temporal degrees of freedom are available. Hence, a single pulse of dimensionality M must have a time duration T and bandwidth W satisfying $M = TW$. Reference [3] explains that Gaussian-state QI can carve $T = M/W$-s duration pulses from the signal and idler outputs of a continuous-wave-pumped parametric downconverter with W-Hz phase-matching bandwidth to obtain the M-dimensional entangled state it needs. It is not clear how to generate the M-dimensional entangled-state pulses that PHE QI needs, but a sequence of $N_T > 10^4$ such pulses are needed for that QI system to realize the Chernoff-bound error probabilities $< 10^{-3}$ from Figure 2 in the moderate-brightness noise, and $N_T > 10^5$ pulses are required in the high-brightness noise. Thus, PHE QI's total required time–bandwidth product is at least 10^8-to-10^{10} times what suffices for Gaussian-state QI to reach $\Pr(e) < 10^{-3}$ in Figure 2's examples.

The final points of comparison between the two QI protocols considered concern the four enormous hurdles, cited in Section 1, that currently preclude finding a realistic target-detection use case for Gaussian-state QI: (i) its need to interrogate one resolution bin at a time; (ii) its need for a quantum memory to store its high time–bandwidth product idler; (iii) its need for extremely high time–bandwidth product radiation to obtain an acceptably low error probability; and (iv) its need for an interferometric measurement. How does PHE QI stack up against these hurdles? There is at least some encouragement in this regard, but so far the overall prospects are pretty poor. In particular, PHE QI still need to interrogate one resolution bin at a time, and it still needs a quantum memory to store its high-dimensionality idler. However, assuming PHE QI's single-pulse idler dimensionality is the same as that of Gaussian-state QI's, its discrete-variable memory may be less complicated to implement than Gaussian-state QI's continuous-variable memory. As has been shown above, however, PHE QI's required single-pulse idler dimensionality is apt to be 10^4-to-10^5 times that of Gaussian-state QI's. Worse, PHE QI's total time–bandwidth product may have to be a factor of 10^8-to-10^{10} times that of Gaussian-state QI, owing to its need to transmit a long sequence of single-photon pulses. A final positive note for PHE QI is that it does not require an interferometric measurement. This phase insensitivity follows from $\hat{\rho}_{RI}^{(0)}$ being diagonal in the number-ket basis, and the anti-normally ordered

characteristic function associated with the joint density operator for the $\{e^{i\phi}\hat{\boldsymbol{a}}_R, \hat{\boldsymbol{a}}_I\}$ modes under hypotheses H_1 being given by Equation (20) for all phase shifts ϕ.

Funding: This research received no external funding.

Data Availability Statement: The original contributions presented in this study are included in the article. Further inquiries can be directed to the author.

Acknowledgments: The author thanks Armanpreet Pannu, Amr S. Helmy, and Hesham El Gamal for early access to their manuscript. He also thanks Roberto Di Candia for alerting him to Ref. [15].

Conflicts of Interest: The author declares no conflicts of interest.

Abbreviations

The following abbreviations are used in this manuscript:

CB	Chernoff bound
GS	Gaussian state
iid	independent, identically distributed
jpdf	joint probability density function
LiDAR	light detection and ranging
LRT	likelihood-ratio test
PHE	Pannu–Helmy–El Gamal
POVM	positive operator-valued measurement
QI	quantum illumination
SP	single-photon
TMSV	two-mode squeezed vacuum

Appendix A. Obtaining $\hat{\rho}_{RI}^{(1)}$ from $\chi_A^{\rho_{RI}^{(1)}}(\boldsymbol{\zeta}_R, \boldsymbol{\zeta}_I)$

In this Appendix, the number-ket matrix elements of $\hat{\rho}_{RI}^{(1)}$ are derived from Equation (22). Let us start by seeking the matrix elements for the first ($m = m'$) line of Equation (22), beginning from

$$ {}_I\langle \mathbf{e}_m|\hat{\rho}_{RI}^{(1)}|\mathbf{e}_m\rangle_I = \int \frac{\mathrm{d}^2\boldsymbol{\zeta}_R}{\pi^M} \int \frac{\mathrm{d}^2\boldsymbol{\zeta}_I}{\pi^M} \chi_A^{\rho_{RI}^{(1)}}(\boldsymbol{\zeta}_R, \boldsymbol{\zeta}_I) e^{-\boldsymbol{\zeta}_R\cdot\hat{\boldsymbol{a}}_R^\dagger} e^{\boldsymbol{\zeta}_R^*\cdot\hat{\boldsymbol{a}}_R} {}_I\langle \mathbf{e}_m|e^{-\boldsymbol{\zeta}_I\cdot\hat{\boldsymbol{a}}_I^\dagger} e^{\boldsymbol{\zeta}_I^*\cdot\hat{\boldsymbol{a}}_I}|\mathbf{e}_m\rangle_I \tag{A1} $$

$$ = \int \frac{\mathrm{d}^2\boldsymbol{\zeta}_R}{\pi^M} \int \frac{\mathrm{d}^2\boldsymbol{\zeta}_I}{\pi^M} \chi_A^{\rho_{RI}^{(1)}}(\boldsymbol{\zeta}_R, \boldsymbol{\zeta}_I) e^{-\boldsymbol{\zeta}_R\cdot\hat{\boldsymbol{a}}_R^\dagger} e^{\boldsymbol{\zeta}_R^*\cdot\hat{\boldsymbol{a}}_R} (1 - |\zeta_{I_m}|^2), \tag{A2} $$

where Equation (A2) follows from the Taylor-series expansions of $e^{-\zeta_{I_m}\hat{a}_{I_m}^\dagger}$ and $e^{\zeta_{I_m}^*\hat{a}_{I_m}}$. Now, substituting from Equation (20) and recognizing that $e^{-\boldsymbol{\zeta}_I^*\cdot\boldsymbol{\zeta}_I}/\pi^M$ is the joint probability density function (jpdf) for the $\{\zeta_{I_m}\}$ to be a collection of M iid circulo-complex Gaussian random variables with mean-squared magnitudes $\langle|\zeta_{I_m}|^2\rangle_{I_m} = 1$, one obtains

$$ {}_I\langle \mathbf{e}_m|\hat{\rho}_{RI}^{(1)}|\mathbf{e}_m\rangle_I = \int \frac{\mathrm{d}^2\boldsymbol{\zeta}_R}{\pi^M} e^{-\boldsymbol{\zeta}_R^*\cdot\boldsymbol{\zeta}_R(N_B+1)} e^{-\boldsymbol{\zeta}_R\cdot\hat{\boldsymbol{a}}_R^\dagger} e^{\boldsymbol{\zeta}_R^*\cdot\hat{\boldsymbol{a}}_R} $$
$$ \times \left\langle \left[1 - \frac{\boldsymbol{\zeta}_I^*\cdot\boldsymbol{\zeta}_I}{M} - \frac{\kappa\boldsymbol{\zeta}_R^*\cdot\boldsymbol{\zeta}_R}{M} + \frac{\kappa|\boldsymbol{\zeta}_R\cdot\boldsymbol{\zeta}_I|^2}{M}\right] \frac{(1 - |\zeta_{I_m}|^2)}{M} \right\rangle_I, \tag{A3} $$

where $\langle\cdot\rangle_I$ denotes expected value over the jpdf $e^{-\boldsymbol{\zeta}_I^*\cdot\boldsymbol{\zeta}_I}/\pi^M$. Complex Gaussian moment factoring then reduces this expression to

$$ {}_I\langle \mathbf{e}_m|\hat{\rho}_{RI}^{(1)}|\mathbf{e}_m\rangle_I = \int \frac{\mathrm{d}^2\boldsymbol{\zeta}_R}{\pi^M} e^{-\boldsymbol{\zeta}_R^*\cdot\boldsymbol{\zeta}_R(N_B+1)} e^{-\boldsymbol{\zeta}_R\cdot\hat{\boldsymbol{a}}_R^\dagger} e^{\boldsymbol{\zeta}_R^*\cdot\hat{\boldsymbol{a}}_R} \frac{(1 - \kappa|\zeta_{R_m}|^2)}{M}. \tag{A4} $$

Next, using the Taylor-series expansions for $e^{-\boldsymbol{\zeta}\cdot\hat{\mathbf{a}}_R^\dagger}$ and $e^{\boldsymbol{\zeta}_R^*\cdot\hat{\mathbf{a}}_R}$, one finds that

$$
\begin{aligned}
{}_R\langle\mathbf{N}|\,{}_m\langle\mathbf{e}_m|\hat{\rho}_{RI}^{(1)}|\mathbf{e}_m\rangle_m\,|\mathbf{N}'\rangle_R = \int\frac{\mathrm{d}^2\boldsymbol{\zeta}_R}{\pi^M}\,e^{-\boldsymbol{\zeta}_R^*\cdot\boldsymbol{\zeta}_R(N_B+1)} \\
\times\left(\bigotimes_{\ell=1}^{M}\sum_{k_\ell=0}^{N_\ell}\sqrt{\frac{N_\ell!}{(N_\ell-k_\ell)!}}\frac{(-\zeta_{R_\ell})^{k_\ell}}{k_\ell!}\,{}_{R_\ell}\langle N_\ell-k_\ell|\right) \\
\times\left(\bigotimes_{\ell'=1}^{M}\sum_{k'_{\ell'}=0}^{N'_{\ell'}}\sqrt{\frac{N'_{\ell'}!}{(N'_{\ell'}-k'_{\ell'})!}}\frac{\zeta_{R_{\ell'}}^{*k'_{\ell'}}}{k'_{\ell'}!}|N'_{\ell'}-k'_{\ell'}\rangle_{R_{\ell'}}\right)\frac{(1-\kappa|\zeta_{R_m}|^2)}{M}.
\end{aligned}
\tag{A5}
$$

The bra-ket inner products in Equation (A5) vanish if $\ell \neq \ell'$, and, because $e^{-\boldsymbol{\zeta}_R^*\cdot\boldsymbol{\zeta}_R(N_B+1)}/[\pi/(N_B+1)]^M$ is the jpdf for the $\{\zeta_{R_m}\}$ to be a collection of M iid circulo-complex Gaussian random variables with mean-squared magnitudes $\langle|\zeta_{R_m}|^2\rangle_{R_m} = 1/(N_B+1)$, complex Gaussian moment factoring implies that only the $k_\ell = k'_\ell$ terms will survive in Equation (A5). The inner products that remain after setting $\ell = \ell'$ and $k'_\ell = k_\ell$, viz., ${}_{R_\ell}\langle N_\ell - k_\ell|N'_\ell - k_\ell\rangle_{R_{\ell'}}$, then vanish unless $N'_\ell = N_\ell$, leading to

$$
\begin{aligned}
{}_R\langle\mathbf{N}|\,{}_m\langle\mathbf{e}_m|\hat{\rho}_{RI}^{(1)}|\mathbf{e}_m\rangle_m\,|\mathbf{N}'\rangle_R = \int\frac{\mathrm{d}^2\boldsymbol{\zeta}_R}{\pi^M}\,e^{-\boldsymbol{\zeta}_R^*\cdot\boldsymbol{\zeta}_R(N_B+1)} \\
\times\left(\bigotimes_{\ell=1}^{M}\delta_{N_\ell N'_\ell}\sum_{k_\ell=0}^{N_\ell}\binom{N_\ell}{k_\ell}\frac{(-|\zeta_{R_\ell}|^2)^{k_\ell}}{k_\ell!}\right)\frac{(1-\kappa|\zeta_{R_m}|^2)}{M}.
\end{aligned}
\tag{A6}
$$

At this point, let us note that

$$
\int\frac{\mathrm{d}^2\zeta_{R_\ell}}{\pi}\,e^{-|\zeta_{R_\ell}|^2(N_B+1)}\sum_{k_\ell=0}^{N_\ell}\binom{N_\ell}{k_\ell}\frac{(-|\zeta_{R_\ell}|^2)^{k_\ell}}{k_\ell!} = \frac{N_B^{N_\ell}}{(N_B+1)^{N_\ell+1}},
\tag{A7}
$$

and

$$
\int\frac{\mathrm{d}^2\zeta_{R_m}}{\pi}\,e^{-|\zeta_{R_m}|^2(N_B+1)}\sum_{k_m=0}^{N_m}\binom{N_m}{k_m}\frac{(-|\zeta_{R_m}|^2)^{k_m+1}}{k_m!} = \frac{(N_m-N_B)N_B^{N_m-1}}{(N_B+1)^{N_m+2}},
\tag{A8}
$$

because the former is the number-ket matrix element ${}_{B_\ell}\langle N_\ell|\hat{\rho}_{B_\ell}^{(0)}|N_\ell\rangle_{B_\ell}$ of the operator-valued inverse Fourier transform of $\chi_A^{\rho_{B_\ell}^{(0)}}(\zeta_{B_\ell})$, and the latter is $\mathrm{d}({}_{B_\ell}\langle N_\ell|\hat{\rho}_{B_\ell}^{(0)}|N_\ell\rangle_{B_\ell})/\mathrm{d}N_B$. Substituting Equations (A7) and (A8) into Equation (A6) then gives us the first line of Equation (22).

Proceeding now to the $m \neq m'$ case, with $m \neq m'$ assumed in all that follows, the starting point is

$$
{}_I\langle\mathbf{e}_m|\hat{\rho}_{RI}^{(1)}|\mathbf{e}_{m'}\rangle_I = \int\frac{\mathrm{d}^2\boldsymbol{\zeta}_R}{\pi^M}\int\frac{\mathrm{d}^2\boldsymbol{\zeta}_I}{\pi^M}\,\chi_A^{\rho_{RI}^{(1)}}(\boldsymbol{\zeta}_R,\boldsymbol{\zeta}_I)e^{-\boldsymbol{\zeta}_R\cdot\hat{\mathbf{a}}_R^\dagger}e^{\boldsymbol{\zeta}_R^*\cdot\hat{\mathbf{a}}_R}\,{}_I\langle\mathbf{e}_m|e^{-\boldsymbol{\zeta}_I\cdot\hat{\mathbf{a}}_I^\dagger}e^{\boldsymbol{\zeta}_I^*\cdot\hat{\mathbf{a}}_I}|\mathbf{e}_{m'}\rangle_I
\tag{A9}
$$

$$
= \int\frac{\mathrm{d}^2\boldsymbol{\zeta}_R}{\pi^M}\int\frac{\mathrm{d}^2\boldsymbol{\zeta}_I}{\pi^M}\,\chi_A^{\rho_{RI}^{(1)}}(\boldsymbol{\zeta}_R,\boldsymbol{\zeta}_I)e^{-\boldsymbol{\zeta}_R\cdot\hat{\mathbf{a}}_R^\dagger}e^{\boldsymbol{\zeta}_R^*\cdot\hat{\mathbf{a}}_R}(-\zeta_{I_m}\zeta_{I_{m'}}^*).
\tag{A10}
$$

Substituting in from Equation (20) and using complex Gaussian moment factoring, the preceding result reduces to

$$ {}_I\langle \mathbf{e}_m|\hat{\rho}_{RI}^{(1)}|\mathbf{e}_{m'}\rangle_I = \frac{\kappa}{M}\int \frac{\mathrm{d}^2\boldsymbol{\zeta}_R}{\pi^M}\, e^{-\boldsymbol{\zeta}_R^*\cdot\boldsymbol{\zeta}_R(N_B+1)} e^{-\boldsymbol{\zeta}_R\cdot\hat{\mathbf{a}}_R^\dagger} e^{-\boldsymbol{\zeta}_R^*\cdot\hat{\mathbf{a}}_R}\langle -\zeta_{R_{m'}}|\zeta_{I_{m'}}|^2\zeta_{R_m}^*|\zeta_{I_m}|^2\rangle_I \quad \text{(A11)} $$

$$ = \frac{\kappa}{M}\int \frac{\mathrm{d}^2\boldsymbol{\zeta}_R}{\pi^M}\, e^{-\boldsymbol{\zeta}_R^*\cdot\boldsymbol{\zeta}_R(N_B+1)} e^{-\boldsymbol{\zeta}_R\cdot\hat{\mathbf{a}}_R^\dagger} e^{-\boldsymbol{\zeta}_R^*\cdot\hat{\mathbf{a}}_R}(-\zeta_{R_{m'}}\zeta_{R_m}^*). \quad \text{(A12)} $$

Using Taylor-series expansions of $e^{-\boldsymbol{\zeta}_R\cdot\hat{\mathbf{a}}_R^\dagger}$ and $e^{\boldsymbol{\zeta}_R^*\cdot\hat{\mathbf{a}}_R}$ in Equation (A12), it follows that

$$ \begin{aligned} {}_R\langle \mathbf{N}|\,{}_I\langle \mathbf{e}_m|\hat{\rho}_{RI}^{(1)}|\mathbf{e}_{m'}\rangle_I\,|\mathbf{N}'\rangle_R &= \frac{\kappa}{M}\int \frac{\mathrm{d}^2\boldsymbol{\zeta}_R}{\pi^M} e^{-\boldsymbol{\zeta}_R^*\cdot\boldsymbol{\zeta}_R(N_B+1)} \\ &\times \left(\bigotimes_{\ell=1}^{M}\sum_{k_\ell=0}^{N_\ell}\sqrt{\frac{N_\ell!}{(N_\ell-k_\ell)!}}\frac{(-\zeta_{R_\ell})^{k_\ell}(-\zeta_{R_{m'}})}{k_\ell!}\,{}_{R_\ell}\langle N_\ell-k_\ell|\right) \\ &\times \left(\bigotimes_{\ell'=1}^{M}\sum_{k'_{\ell'}=0}^{N'_{\ell'}}\sqrt{\frac{N'_{\ell'}!}{(N'_{\ell'}-k'_{\ell'})!}}\frac{\zeta_{R_{\ell'}}^{*k'_{\ell'}}\zeta_{R_m}^*}{k'_{\ell'}!}\,|N'_{\ell'}-k'_{\ell'}\rangle_{R_{\ell'}}\right). \end{aligned} \quad \text{(A13)} $$

Complex Gaussian moment factoring now implies that for $\ell,\ell' \neq m,m'$ only the $\ell=\ell'$, $k_\ell = k'_\ell$ terms survive, in which case the bra-ket inner product shows that $N_\ell = N'_\ell$ also holds, leaving us with

$$ \begin{aligned} {}_R\langle \mathbf{N}|\,{}_I\langle \mathbf{e}_m|\hat{\rho}_{RI}^{(1)}|\mathbf{e}_{m'}\rangle_I\,|\mathbf{N}'\rangle_R &= \frac{\kappa}{M}\left(\prod_{\substack{\ell=1\\ \ell\neq m,m'}}^{M}\frac{N_B^{N_\ell}\delta_{N_\ell N_{\ell'}}}{(N_B+1)^{N_\ell+1}}\right) \\ &\times \int\frac{\mathrm{d}^2\zeta_{R_m}}{\pi}\int\frac{\mathrm{d}^2\zeta_{R_{m'}}}{\pi}\, e^{-(|\zeta_{R_m}|^2+|\zeta_{R_{m'}}|^2)(N_B+1)} \\ &\times \left(\sum_{k_m=0}^{N_m}\sqrt{\frac{N_m!}{(N_m-k_m)!}}\frac{(-\zeta_{R_m})^{k_m}}{k_m!}\,{}_{R_m}\langle N_m-k_m|\right) \\ &\times \left(\sum_{k_{m'}=0}^{N_{m'}}\sqrt{\frac{N_{m'}!}{(N_{m'}-k_{m'})!}}\frac{(-\zeta_{R_{m'}})^{k_{m'}+1}}{k_{m'}!}\,{}_{R_{m'}}\langle N_{m'}-k_{m'}|\right) \\ &\times \left(\sum_{k'_{m'}=0}^{N'_{m'}}\sqrt{\frac{N'_{m'}!}{(N'_{m'}-k'_{m'})!}}\frac{\zeta_{R_{m'}}^{*k'_{m'}}}{k'_{m'}!}\,|N'_{m'}-k'_{m'}\rangle_{R_{m'}}\right) \\ &\times \left(\sum_{k'_m=0}^{N'_m}\sqrt{\frac{N'_m!}{(N'_m-k'_m)!}}\frac{\zeta_{R_m}^{*(k'_m+1)}}{k'_m!}\,|N'_m-k'_m\rangle_{R_m}\right). \end{aligned} \quad \text{(A14)} $$

The only terms that survive the remaining complex Gaussian moment factoring are those for which $k_m = k'_m + 1$ and $k_{m'} + 1 = k'_{m'}$, and these conditions imply that the only terms that survive after evaluation of the remaining bra-ket inner products are those for which $N_m = N'_m + 1$ and $N_{m'} + 1 = N'_{m'}$, giving us

$$
\begin{aligned}
{}_R\langle \mathbf{N}|\,{}_I\langle \mathbf{e}_m|\hat{\rho}_{RI}^{(1)}|\mathbf{e}_{m'}\rangle_I\,|\mathbf{N}'\rangle_R = \frac{\kappa}{M}&\left(\prod_{\substack{\ell=1\\ \ell\neq m,m'}}^{M}\frac{N_B^{N_\ell}\delta_{N_\ell N_{\ell'}}}{(N_B+1)^{N_\ell+1}}\right)\\
&\times\int\frac{\mathrm{d}^2\zeta_{R_m}}{\pi}\int\frac{\mathrm{d}^2\zeta_{R_{m'}}}{\pi}\,e^{-(|\zeta_{R_m}|^2+|\zeta_{R_{m'}}|^2)(N_B+1)}\\
&\times\left(\sum_{k'_m=0}^{N'_m}\binom{N'_m}{k'_m}\frac{\sqrt{N'_m+1}\,(-|\zeta_{R_m}|^2)^{k'_m+1}}{(k'_m+1)!}\right)\\
&\times\left(\sum_{k_{m'}=0}^{N_{m'}}\binom{N_{m'}}{k_{m'}}\frac{\sqrt{N_{m'}+1}\,(-|\zeta_{R_{m'}}|^2)^{k_{m'}+1}}{(k_{m'}+1)!}\right)\delta_{N_m(N'_m+1)}\delta_{N'_m(N_{m'}+1)}.
\end{aligned}
\tag{A15}
$$

To complete the derivation, the ζ_{R_m} and $\zeta_{R_{m'}}$ integrations are performed, resulting in

$$
\begin{aligned}
{}_R\langle \mathbf{N}|\,{}_I\langle \mathbf{e}_m|\hat{\rho}_{RI}^{(1)}|\mathbf{e}_{m'}\rangle_I\,|\mathbf{N}'\rangle_R = \frac{\kappa}{M}&\left(\prod_{\substack{\ell=1\\ \ell\neq m,m'}}^{M}\frac{N_B^{N_\ell}\delta_{N_\ell N_{\ell'}}}{(N_B+1)^{N_\ell+1}}\right)\left(\sum_{k'_m=0}^{N'_m}\binom{N'_m}{k'_m}\frac{(-1)^{k'_m+1}}{(N_B+1)^{k'_m+2}}\right)\\
\times\left(\sum_{k_{m'}=0}^{N_{m'}}\binom{N_{m'}}{k_{m'}}\frac{(-1)^{k_{m'}+1}}{(N_B+1)^{k_{m'}+2}}\right)&\sqrt{(N'_m+1)(N_{m'}+1)}\,\delta_{N_m(N'_m+1)}\delta_{N'_m(N_{m'}+1)},
\end{aligned}
\tag{A16}
$$

after which the binomial sums are done to obtain the final result,

$$
\begin{aligned}
{}_R\langle \mathbf{N}|\,{}_I\langle \mathbf{e}_m|\hat{\rho}_{RI}^{(1)}|\mathbf{e}_{m'}\rangle_I\,|\mathbf{N}'\rangle_R = \frac{\kappa}{M}&\left(\prod_{\substack{\ell=1\\ \ell\neq m,m'}}^{M}\frac{N_B^{N_\ell}\delta_{N_\ell N_{\ell'}}}{(N_B+1)^{N_\ell+1}}\right)\\
&\times\frac{N_B^{N'_m+N_{m'}}\sqrt{(N'_m+1)(N_{m'}+1)}}{(N_B+1)^{N'_m+N_{m'}+4}}\,\delta_{N_m(N'_m+1)}\delta_{N'_m(N_{m'}+1)},
\end{aligned}
\tag{A17}
$$

which verifies the second and third lines of Equation (22).

Appendix B. First-Order Corrections to Section 4's p_F and p_D Approximations

This Appendix assesses the accuracies of the p_F and p_D approximations from Equations (26) and (36). Those formulas relied on approximating $1/(|\tilde{\mathbf{N}}|+M-\delta_{k0})$, for $k=0$ and 1, respectively, by the $n=0$ term of

$$
\frac{1}{|\tilde{\mathbf{N}}|+M-\delta_{k0}}=\frac{1}{M(N_B+1)-\delta_{k0}}\left[\sum_{n=0}^{\infty}\left(\frac{-|\Delta\tilde{\mathbf{N}}|}{M(N_B+1)-\delta_{k0}}\right)^n\right],
\tag{A18}
$$

where $\Delta\tilde{\mathbf{N}}\equiv(\Delta\tilde{N}_1,\Delta\tilde{N}_2,\ldots,\Delta\tilde{N}_M)$, with $\Delta\tilde{N}_m\equiv\tilde{N}_m-N_B$, being the fluctuating part of $\tilde{\mathbf{N}}$, and $|\Delta\tilde{\mathbf{N}}|\equiv\sum_{m=1}^{M}\Delta\tilde{N}_m$.

The bracketed term in Equation (A18) is a stochastic Taylor series. Assuming $M\gg 1$, as is the case for PHE QI, the mean-to-standard-deviation ratio of $x\equiv|\tilde{\mathbf{N}}|+M-\delta_{k0}$ satisfies

$$
\frac{\mathbb{E}(x)}{\sqrt{\mathrm{Var}(x)}}=\frac{M(N_B+1)-\delta_{k0}}{\sqrt{MN_B(N_B+1)}}\gg 1.
\tag{A19}
$$

for all N_B in both the p_F and p_D calculations. Thus, the $n=1$ terms from Equation (A18) are included to see how much that changes the results from Section 4.

Including the $n = 1$ term from Equation (A18) implies that the false-alarm probability approximation becomes $N_B/[M(N_B+1)-1] - \Delta_F$ where

$$\Delta_F \equiv \frac{1}{M}\sum_{m=1}^{M}\sum_{\tilde{\mathbf{N}}}\Pr(\tilde{\mathbf{N}})\frac{\tilde{N}_m|\Delta\tilde{\mathbf{N}}|}{[M(N_B+1)-1]^2}, \tag{A20}$$

with $\Pr(\tilde{\mathbf{N}}) = \prod_{m=1}^{M} N_B^{N_m}/(N_B+1)^{N_m+1}$. It is now a straightforward calculation to show that

$$\Delta_F = \frac{N_B(N_B+1)}{[M(N_B+1)-1]^2}, \tag{A21}$$

so that including the first-order correction gives us

$$p_F \approx \frac{N_B}{M(N_B+1)-1}\left(1 - \frac{N_B+1}{M(N_B+1)-1}\right). \tag{A22}$$

This result shows that, for all N_B, the first-order correction has virtually no effect on the false-alarm probability approximation when $M \gg 1$.

This paper's last task is to obtain the detection-probability approximation when the $n = 1$ term from Equation (A18) is included. Here the starting point is $p_D \approx (M\kappa + N_B)/M(N_B+1) - \Delta_D$, where

$$\Delta_D = \sum_{\tilde{\mathbf{N}}}\sum_{m=1}^{M}\sum_{m'=1}^{M}\frac{|\Delta\tilde{\mathbf{N}}|\sqrt{(\tilde{N}_m+1)(\tilde{N}_{m'}+1)}}{[M(N_B+1)]^2}\,{}_R\langle \mathbf{e}_m + \tilde{\mathbf{N}}|\hat{\rho}_{RI}^{(1)}|\mathbf{e}_{m'} + \tilde{\mathbf{N}}\rangle_R. \tag{A23}$$

As was done in Section 4 for the $n = 0$ detection-probability approximation, the $m = m'$ and $m \neq m'$ terms in Δ_D are calculated separately. For $\Delta_D^{(m=m')}$:

$$\begin{aligned}\Delta_D^{(m=m')} &= \frac{1}{M}\sum_{\tilde{\mathbf{N}}}\sum_{m=1}^{M}\frac{|\Delta\tilde{\mathbf{N}}|(\tilde{N}_m+1)}{[M(N_B+1)]^2}\left(\prod_{\substack{\ell=1\\ \ell\neq m}}^{M}\frac{N_B^{\tilde{N}_\ell}}{(N_B+1)^{\tilde{N}_\ell+1}}\right)\frac{N_B^{\tilde{N}_m+1}}{(N_B+1)^{\tilde{N}_m+2}} \\ &\quad\times\left(1 - \frac{\kappa}{N_B+1} + \frac{\kappa(\tilde{N}_m+1)}{N_B(N_B+1)}\right) \qquad \text{(A24)} \\ &= \frac{N_B(3\kappa+N_B)}{[M(N_B+1)]^2} \ll p_D^{(m=m')}, \qquad \text{(A25)}\end{aligned}$$

for $M \gg N_B + 1$, as will be the case in the quantum-advantage regime, cf. Figure 1. Finally, for $m \neq m'$, one has

$$\begin{aligned}\Delta_D^{(m\neq m')} &= \frac{\kappa}{M}\sum_{m=1}^{M}\sum_{\substack{m'=1\\ m'\neq m}}^{M}\sum_{\tilde{N}_m=0}^{\infty}\sum_{\tilde{N}_{m'}=0}^{\infty}\frac{N_B^{\tilde{N}_m+\tilde{N}_{m'}}}{(N_B+1)^{\tilde{N}_m+\tilde{N}_{m'}+4}}\frac{|\Delta\tilde{\mathbf{N}}|(\tilde{N}_m+1)(\tilde{N}_{m'}+1)}{[M(N_B+1)]^2} \qquad \text{(A26)} \\ &= \frac{\kappa(M-1)N_B^2}{[M(N_B+1)]^2} \ll p_D^{(m\neq m')}, \qquad \text{(A27)}\end{aligned}$$

for $M \gg N_B + 1$, as will be the case in the quantum-advantage regime, cf. Figure 1. Putting together Equations (A25) and (A27) shows that the first-order correction to the p_D approximation from Section 4 has essentially no effect.

References

1. Skolnik, M.I. *Introduction to Radar Systems*; McGraw-Hill Companies, Inc.: New York, NY, USA, 2001. Available online: https://archive.org/details/254439180 (accessed on 1 February 2025).
2. Louisell, W.H. *Quantum Statistical Properties of Radiation*; John Wiley & Sons, Inc.: New York, NY, USA, 1973. Available online: https://www.scribd.com/document/443096749/epdf-pub-quantum-statistical-properties-of-radiation-wiley-pdf (accessed on 1 February 2025).
3. Shapiro, J.H. The quantum illumination story. *IEEE Aerosp. Electron. Sys. Mag.* **2020**, *35(4)*, 8–20. [CrossRef]
4. Sorelli, G.; Treps, N.; Grosshans, F.; Boust, F. Detecting a target with quantum entanglement. *IEEE Aerosp. Electron. Mag.* **2022**, *37(5)*, 68–90. [CrossRef]
5. Karsa, A.; Fletcher, A.; Spedalieri, G.; Pirandola, S. Quantum illumination and quantum radar: A brief overview. *Rep. Prog. Phys.* **2024**, *87*, 094001. [CrossRef] [PubMed]
6. Lloyd, S. Enhanced sensitivity of photodetection via quantum illumination. *Science* **2008**, *321*, 1463–1465. [CrossRef] [PubMed]
7. Shapiro, J.H.; Lloyd, S. Quantum illumination versus coherent-state target detection. *New J. Phys.* **2009**, *11*, 063045. [CrossRef]
8. Tan, S.-H.; Erkmen, B.I.; Giovannetti, V.; Guha, S.; Lloyd, S.; Maccone, L.; Pirandola, S.; Shapiro, J.H. Quantum illumination with Gaussian states. *Phys. Rev. Lett.* **2008**, *101*, 253601. [CrossRef] [PubMed]
9. Shapiro, J.H.; Guha, S.; Erkmen, B.I. Ultimate channel capacity of free-space optical communications. *J. Opt. Netw.* **2005**, *5*, 501–516. [CrossRef]
10. Barzanjeh, S.; Guha, S.; Weedbrook, C.; Vitali, D.; Shapiro, J.H.; Pirandola, S. Microwave quantum illumination. *Phys. Rev. Lett.* **2015**, *114*, 080503. [CrossRef] [PubMed]
11. Zhang, Z.; Mouradian, S.; Wong, F.N.C.; Shapiro, J.H. Entanglement-enhanced sensing in a lossy and noisy environment. *Phys. Rev. Lett.* **2015**, *114*, 110506. [CrossRef] [PubMed]
12. Assouly, R.; Dassonneville, R.; Peronnin, T.; Bienfait, A.; Huard, B. Quantum advantage in microwave quantum radar. *Nat. Phys.* **2023**, *18*, 1418–1422. [CrossRef]
13. Pannu, A.; Helmy, A.S.; El Gamal, H. Quantum illumination with high-dimensional Bell states. *Phys. Rev. A* **2024**, *110*, L050603. [CrossRef]
14. Nair, R.; Gu, M. Fundamental limits of quantum illumination. *Optica* **2020**, *7*, 771–774. [CrossRef]
15. Di Candia, R.; Yiğitler, H.; Paraoanu, G.S.; Jäntti, R. Two-way covert quantum communication in the microwave regime. *PRX Quantum* **2021**, *2*, 020316. [CrossRef]
16. Nielsen, M.A.; Chuang, I.L. *Quantum Computation and Quantum Information*; Cambridge University: New York, NY, USA, 2010. [CrossRef]